Mathematical Modelling and Analysis
Volume 15 Number 1, 2010, pages 23–38
Doi:10.3846/1392-6292.2010.15.23-38

ISSN 1392-6292 print
ISSN 1648-3510 online
www.vgtu.lt/mma/

Numerical Analysis of Laser Diode Longitudinally Pumped Solid-State Laser Generation Dynamics Using Traveling Wave Model

A.S. Dement'ev[2], R. Čiegis[1], I. Laukaitytė[1] and N. Slavinskis[2]

[1] *Vilnius Gediminas Technical University ,*
[2] *Institute of Physics*
[1] Saulėtekio av. 11, LT-10223, Vilnius, Lithuania,
[2] Savanoriu av. 231, Vilnius, Lithuania
E-mail(*corresp.*): {rc, ing}@fm.vgtu.lt,
E-mail: aldement@ktl.mii.lt; nslavinskis@ar.fi.lt

Received December 2, 2009; revised December 24, 2009; published online February 15, 2010

Abstract. A detailed theoretical model for the description of generation dynamics of diode laser longitudinally pumped solid-state lasers with active and/or passive Q-switching using traveling wave approach is presented. The results of numerical simulations and analysis show that the distribution of generated laser pulse intensity and the other laser parameters along the resonator is very inhomogeneous. Therefore, the widely used point laser model cannot give accurate results when inside the resonator there are active or passive elements which lead to the strong modulation of the generated pulse intensities.

Keywords: solid-state lasers, mathematical modelling, traveling wave model, generation dynamics, numerical analysis, computational experiments.

AMS Subject Classification: 65C20; 78A60.

1 Introduction

Solid-state lasers (SSL) were developed more than four decades ago and they still remain a very actual area of research and applications [7, 30] because of several innovations in technology, and the pace of SSL development is accelerating. SSL have capabilities which no other type of laser has. The most important change over the past few decades is the development of high power laser diode (LD) sources, which have been specially developed for SSL pumping [2]. Newly developed LD allows direct in-band pumping into the emitting levels

[28]. Direct upper laser level pumping leads to lower heat dissipation and offers significant system benefits from an efficiency perspective [3]. SSL utilizing simple end-pumped rod configurations have found their way into many commercial laser systems as such pumping architecture allows to excite selectively the fundamental laser mode, thus it provides low threshold pump powers and high optical efficiencies.

Described technological development of SSL requires a detailed modelling of such end-pumped SSL taking into account more parameters of active laser medium, pump sources and resonator architecture. But for modelling of generation dynamics the so called point laser model (PLM) is still widely used (see [9, 14, 16, 30, 35] and references therein). Due to significant mathematical difficulties traveling wave model (TWM) is rarely used for laser generation modelling [4, 8, 11, 20, 32, 33]. This model is more often used for numerical analysis of fiber [11, 33] and semiconductor [12, 20, 32] lasers. This is quite natural, since fiber lasers (FL) have a long active media, and semiconductor lasers (SL) have high pulse repetition rate. Therefore the duration of SL generated pulses is not far lower than the period of pulse repetition. Due to this reason the TWM does not require very lengthy simulations for these lasers. For a more standard SSL this model was used in [4, 8] only for simulation of giant pulse generation during enough short period of time when threshold of population inversion is practically achieved. It should be noted that for the generation of smooth pulses the external seeding is required in this situation. The TWM can be successfully used for short pulse amplification modelling in the multipass amplifiers [5, 10, 25]. However it should be noted that very often the TWM is used in a simplified version, only during initial stage of problem investigation for setting grounds of common strongly simplified models which are used in subsequent studies [9, 18, 19, 24, 27, 32].

In this paper, we have applied TWM for the numerical analysis of laser diode end-pumped passively and/or actively Q-switched solid-state minilasers. The Stark splitting of the lasing levels into sublevels, the finite lifetimes of excited levels, excited state absorption in active elements (AE) and saturated absorber (SA) and many other parameters of AE, SA and pump sources were taken into account. The full system of equations with corresponding initial and boundary conditions was numerically solved using the algorithms developed in [11, 23]. The obtained results are compared with the known theoretical and experimental data of SSL generation dynamics.

2 Model Description

The fundamentals of the TWM for theoretical analysis of SSL generation dynamics in the Q-switched resonator are described with a different degree of completeness in monographs [1, 21, 26, 30, 31, 36]. When describing the generation dynamics of Q-switched lasers, two approximate approaches are most often used: considering the laser as a lengthy system within the intensity traveling plane wave model and the laser as a dimensionless system within the PLM. For validation of the last model, the technique of spatial averaging of TWM equations in partial derivatives over the resonator length is often used

[16, 26, 31]. It is a very complicated task to take into account the complex spatial profiles of laser resonator modes. Therefore, two simplified methods are used for these purposes: Gaussian mode approach in combination with rate equations and beam propagation method based on the Huygens-Fresnel approximation of the diffraction theory [6]. Recently a new approach has been developed [34] in which the common set of rate equations is extended to a set of rate equation for the individual transverse modes being excited in the cavity. However, it should be noted that forward and backward traveling waves do not exist in these simplified methods. For example, under assumption that mode shapes do not change in time, only energy density of the incoherent superposition of the individual modes is used in rate equations [34]. Thus, only the usage of TWM can provide the knowledge about intracavity dynamics during the pulse generation time. But the general case of traveling waves with complex transverse shape requires a very complicated for numerical analysis. Therefore in this paper we use the approximation of the forward and backward traveling plane waves. Neglecting the interference of the forward and backward traveling waves one can obtain equations for traveling intensity waves for the case when these intensities and population inversion are changed insignificantly during the phase relaxation time T_2 [1, 17, 21, 26, 31, 36].

The scheme of SSL resonator with plane mirrors $M_{1,2}$ is presented in Fig. 1. The active element (AE), active (aQ-sw) and/or passive (pQ-sw) Q-switchers are placed inside the Fabry-Perrot resonator. Modeling the evolution of an optical field intensities $I_i^{\pm}$ in the laser elements is based on the general radiation transport equations

$$\hat{L}_i^{\pm} I_i^{\pm} = F_i^{\pm}(z,t),$$

where $\hat{L}_i^{\pm} = \dfrac{1}{v_i^{\pm}} \dfrac{\partial}{\partial t} \pm \dfrac{\partial}{\partial z}$ are the radiation transfer operators in positive (+) and negative (-) propagation directions with respect to the z axis, $v_i^{\pm}$ are group velocities, $F_i^{\pm}(z,t)$ are the functions, depending on variables z, t through the corresponding intensities, population densities, etc., see [1, 21, 26, 31, 36]. To find the form of $F_i^{\pm}(z,t)$ for the concrete element of the resonator the detailed description of the radiation interaction with matter inside this element is necessary.

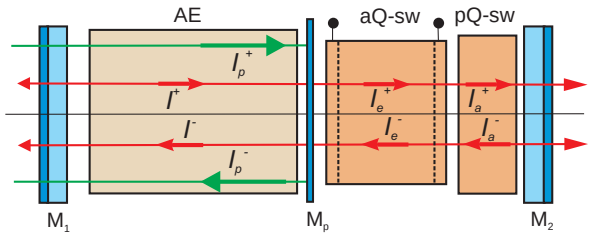

Figure 1. Scheme of an actively and (or) passively Q-switched SSL.

Active element. In order to characterize laser materials, different models have been developed to describe various processes in AE. Most of these models are based on the rate equations accounting for the changes in the level populations. The generalized scheme of Nd:YAG (Neodymium-doped Yttrium Aluminium Garnet) energy levels and possible transitions are presented in Fig. 2. Closely spaced energy levels (here measured in cm^{-1}) with the same angular momentum quantum numbers are grouped into four manifolds: ${}^4I_{9/2}$ is the ground (g) state manifold, ${}^4I_{11/2}$ and ${}^4F_{3/2}$ are the lower (l) and upper (u) laser working manifolds, and many other levels with higher energies form the so called pump (p) levels [36]. Therefore, Nd:YAG laser is a classical type of a four-level laser system. Close spacing of the energy of the Stark sublevels in each manifold provides a rapid thermalization times of the order of a picosecond. The fractional population of each energy level j with energy $E_{i,j}$ in the manifold $i = g, l, u, p$ is described by a Boltzmann or thermal occupation factor

$$f_{i,j}(T) = \exp\left(\frac{-E_{i,j}}{k_B T}\right) / Z_i,$$

where the sum $Z_i(T) = \sum_{j\in i} \exp\left(-E_{i,j}/k_B T\right)$ is over all levels in manifold i, k_B is the Boltzmann constant, T is the temperature. For example, these occupation factors calculated at $300K$ for the ground manifold are equal to $f_{1,1} = 0.464$, $f_{1,2} = 0.246$, $f_{1,3} = 0.178$, $f_{1,4} = 0.104$, $f_{1,5} = 0.078$. The changes of the temperature along the AE are neglected, and the occupation factors are assumed to be constant in the following calculations. The relax-

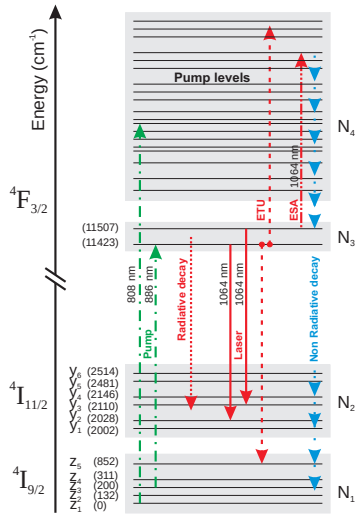

Figure 2. A detailed view of the Nd:YAG energy levels and transitions in the TWM.

ation of electrons from the pump levels manifold to the upper laser manifold is fast compared to the rates of optical pump absorption and typical duration of generated giant laser pulses (it is assumed that non radiative decay time τ_{43} is less than 1 ns).

Absorption of the forward (+) and backward (-) pump intensities $I_{p1}^{\pm}(z,t)$ due to the transitions from the ground manifold to the pump manifold (for example, pump wavelength is equal to $\lambda_p = 808$ nm in Fig. 2) is described by the transport equation

$$\frac{1}{v_p}\frac{\partial I_{p1}^{\pm}}{\partial t} \pm \frac{\partial I_{p1}^{\pm}}{\partial z} = \sigma_p^{(14)} \left(f_{p4}^{(14)} N_4 - f_{p1}^{(14)} N_1 \right) I_{p1}^{\pm} - \alpha_{p1}^{\pm} I_{p1}^{\pm}, \qquad (2.1)$$

where v_p is the group velocity of pump wave in AE, $\sigma_p^{(14)}$ is the pump absorption cross-section for the transition between these manifolds, N_4 and N_1 are the population densities of the pump and ground manifolds, $f_{p1}^{(14)}$ and $f_{p4}^{(14)}$ are corresponding occupation factors and $\alpha_{p1}^{\pm}$ are non resonant pump absorption coefficients. It should be noted that the values of $\sigma_p^{(14)}$, $f_{p1}^{(14)}$ and $f_{p4}^{(14)}$ depend on the set of concrete levels participating in this transition. Direct pumping ($\lambda_p = 886$ nm in Fig. 2) into the upper laser manifold [28] is described by the equation

$$\frac{1}{v_p}\frac{\partial I_{p2}^{\pm}}{\partial t} \pm \frac{\partial I_{p2}^{\pm}}{\partial z} = \sigma_p^{(13)} \left(f_{p3}^{(13)} N_3 - f_{p1}^{(13)} N_1 \right) I_{p2}^{\pm} - \alpha_{p2}^{\pm} I_{p2}^{\pm}. \qquad (2.2)$$

Here the notations are the analogous to Eq. (2.1), and the note about the values of the parameters is the same.

The evolution of the laser intensity is described by the equation

$$\frac{1}{v}\frac{\partial I^{\pm}}{\partial t} \pm \frac{\partial I^{\pm}}{\partial z} = \sigma \left(f_3 N_3 - f_2 N_2 \right) I^{\pm} - \sigma_{esa} f_3^{(esa)} N_3 I^{\pm} - \alpha^{\pm} I^{\pm} + \varepsilon^{\pm} \frac{N_3}{\tau_{32}}, \qquad (2.3)$$

where v is the group velocity of laser wave in AE, N_3 and N_2 are the population densities of the upper and lower laser manifolds, $\alpha^{\pm}$ are coefficients of the non resonant absorption of laser intensity. Due to the fact that two simultaneous laser transitions in Nd:YAG [36] are realized with practically the same wavelength $\lambda_L = 1064$ nm, the generated laser intensities $I^{\pm}$ cause both transitions. Therefore, in (2.3) we use the effective cross section $\sigma = 8.8 \cdot 10^{-19}$ cm^2 [36] and the occupation factors

$$f_2 := \frac{\sigma_{em}^{(2)} f_{2,2} + \sigma_{em}^{(2)} f_{2,3}}{\sigma} = 0.213, \quad f_3 := \frac{\sigma_{em}^{(1)} f_{3,1} + \sigma_{em}^{(1)} f_{3,2}}{\sigma} = 0.452,$$

which are found from the equation using emission cross sections $\sigma_{em}^{(1)}$=$1.9 \cdot 10^{-19}$ cm^2 and $\sigma_{em}^{(2)} = 7.1 \cdot 10^{-19}$ cm^2 [36]. The possibility of excited state absorption is taken into account by the cross section σ_{esa} and the effective occupation factor $f_3^{(esa)}$. Spontaneous emission is described by the term [18]

$$\varepsilon^{\pm} = \Delta\Omega hc/(4\pi\lambda_f),$$

where $\Delta\Omega$ is the spontaneous emission acceptance solid angle, h is the Planck constant, c is the velocity of light in vacuum, λ_f is the energy-averaged fluorescence wavelength of the spontaneous transition.

Rate equations for the population densities of the manifolds are

$$\frac{\partial N_4(z,t)}{\partial t} = -\beta_p^{(14)}\sigma_p^{(14)}\left(f_{p4}^{(14)}N_4 - f_{p1}^{(14)}N_1\right)\left(I_{p1}^{+}+I_{p1}^{-}\right) + \beta_\lambda\sigma_{esa}f_3^{(esa)}N_3(I^+ + I^-) + \beta_{up}N_3^2 - N_4/\tau_{43}, \tag{2.4}$$

$$\frac{\partial N_3(z,t)}{\partial t} = -\beta_p^{(13)}\sigma_p^{(13)}\left(f_{p3}^{(13)}N_3 - f_{p1}^{(13)}N_1\right)\left(I_{p2}^{+}+I_{p2}^{-}\right) - \beta_\lambda\sigma\left(f_3N_3 - f_2N_2\right)(I^+ + I^-) - \beta_\lambda\sigma_{esa}f_3^{(esa)}N_3(I^+ + I^-) - 2\beta_{up}N_3^2 - \beta_{ase}N_3^2 + N_4/\tau_{43} - N_3/\tau_{32} \tag{2.5}$$

$$\frac{\partial N_2(z,t)}{\partial t} = \beta_\lambda\sigma\left(f_3N_3 - f_2N_2\right)\left(I^+ + I^-\right) + N_3/\tau_{32} - N_2/\tau_{21}, \tag{2.6}$$

$$N_1 + N_2 + N_3 + N_4 = N_{Nd}. \tag{2.7}$$

Here $\beta_L = \lambda/hc$, $\beta_p^{(14)} = \lambda_{p1}/hc$ and $\beta_p^{(13)} = \lambda_{p2}/hc$ are the coefficients needed for transition from the photon numbers densities to the intensity values, $h = 6.626 \cdot 10^{-34}$Js. The nonlinear terms with coefficients β_{ase} and β_{up} could be caused by amplified spontaneous emission (ASE) or by upconversion [22]. Energy-transfer-upconversion (ETU) is an energy-transfer process between two neighbouring ions in the upper laser level (Fig. 2). ETU converts two excited ions into one excited and one ion of ground state. During the return of highly excited ion from pump levels to the upper laser level extra heat is generated. It should be noted that ESA in Nd:YAG laser at wavelength $\lambda_L = 1064$ nm can be originated due to transitions from both Stark levels of upper laser working manifold. Therefore, the effective occupation factor $f_3^{(esa)}$ is used in Eqs. (2.4) and (2.5). Appropriate relaxation times τ_{43}, τ_{32} and τ_{21} between the manifolds are introduced in rate equations. N_{Nd} is the concentration of Nd ions in the YAG host.

In numerical simulations, it is convenient to use a dimensionless form of the equations. For Q-switched SSL with short resonator and pulse duration in the nanosecond region the following normalization parameters are suitable: $z_0 = 1$ cm, $t_0 = 1$ ns, $I_0 = 1$ GW/cm^2, $\sigma_0 = 10^{-19}$ cm^2, $N_0 = 10^{19}$ cm^{-3}. Calculation of the dimensionless parameters from the known parameters is a very simple procedure: for all space-time variables $\bar{A}(\bar{z},\bar{t}) = A(z,t)/A_0$, where $\bar{z} = z/z_0$ and $\bar{t} = t/t_0$. For the other parameters normalization depends on the physical meaning of the parameter and it is also very simple. For example, $\bar{\alpha}^{\pm} = \alpha^{\pm}z_0$, $\bar{\varepsilon}^{\pm} = \varepsilon^{\pm}N_0/(I_0t_0)\bar{\beta}_\lambda = \sigma_0I_0t_0\lambda/(hc)$ and similar expressions are valid for the other analogous parameters. Taking into account that the refractive index of YAG crystal n_0 depends insignificantly on the wavelength and on the concentration of Nd and Cr ions, the group velocities in AE and SA are assumed to be equal to $v = v_p = v_a = c/n_0$ and $\bar{v} = ct_0/n_0z_0$. For convenience in the following text we will use the same notation (without upper hyphen) for normalized variables and parameters.

Saturable absorber. Passive Q-switching (PQS) of Nd:YAG lasers is commonly organized by using Cr:YAG crystals. The simplified scheme of energy

levels and absorption transitions in the Cr:YAG Q-switcher is presented in Fig. 3. Absorption of laser radiation from ground and excited states are usually realized during the PQS process.

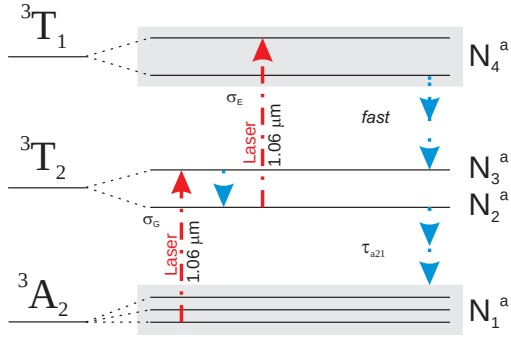

Figure 3. A scheme of energy levels and transitions in Cr:YAG crystal.

The relaxation time from the excited state is assumed to be very fast, and the relaxation time from metastable lower sublevel is long enough. A more detailed analysis of transition times in five-level scheme of Cr:YAG can be found in [13]. The radiation transport equation and the rate equations for population densities are defined as

$$\frac{1}{v_a}\frac{\partial I_a^{\pm}}{\partial t} \pm \frac{\partial I_a^{\pm}}{\partial z} = -\Big(\sigma_g \sum_j f_j(\theta) N_{a1}^{(j)} + \sigma_e \sum_j f_j(\theta) N_{a2}^{(j)}\Big) I_a^{\pm} - \alpha_a I_a^{\pm}, \quad (2.8)$$

$$\frac{\partial N_{a1}^{(j)}}{\partial t} = -\beta_a \beta_\lambda \sigma_g (I_a^+ + I_a^-) f_j(\theta) N_{a1}^{(j)} + N_{a2}^{(j)}/\tau_{a21},$$

$$N_{a1}^{(j)} + N_{a2}^{(j)} = N_{Cr},$$

Here σ_g and σ_e are the cross sections of generated radiation absorption from the ground and excited levels, α_a is non resonant absorption coefficient, $N_{e1,2}^{(j)}$ is the population densities of Cr^{+4} dipoles orientated along the unit vector $\hat{\mathbf{j}}$ of crystal axis, $f_j(\theta) = (\hat{\mathbf{j}}\hat{\mathbf{e}})^2$ is the interaction coefficient of laser radiation polarized along the unit vector $\hat{\mathbf{e}}$ with the appropriate Cr^{+4} dipoles. The influence of Cr:YAG crystal orientation on the generation dynamics was studied in [14, 15, 16] using PLM. Recently analogous generalization of orientation of Nd^{3+} dipoles was proposed for Nd:YAG laser medium [29]. In this paper for the simplicity we will use only parallel orientation of polarization with crystal axis $\Big(f_j(\theta) = (\hat{\mathbf{j}}\hat{\mathbf{e}})^2 \equiv 1\Big)$ and will not take into account the same possibility for Nd^{3+} dipoles. Coefficient β_a accounts for the possibility of changing the transverse area of laser beam in pQ-sw as compared with an AE.

Active Q-switch. Active Q-switch (AQS) of resonator can be realized experimentally by different methods. Acousto-optical (AO) and electro-optical

(EO) modulators are commonly used for Q-switching. We have modelled both of them by the prescribed temporal transmittance changes

$$I^{\pm}(Z_Q \pm 0, t) = T_Q^{(\pm)}(Z_Q, t) I^{\pm}(Z_Q, t),$$

where Z_Q is the switching point. The transmittance $T_Q^{(\pm)}(Z_Q, t)$ can be different for forward and backward traveling waves. It should be noted that for TWM of laser all functions should be smooth enough in space-time coordinates. To be able to describe active quality modulation of the resonator at pulse repetition regime we have used the transmittance function

$$T_Q^{(\pm)}(z_Q, \bar{t}) = \begin{cases} T_{low}^{\pm}, & 0 \le \bar{t} \le t_{m1}, \\ T_{low}^{\pm} + (T_{high}^{\pm} - T_{low}^{\pm}) \left(\frac{\bar{t} - t_{m1}}{\Delta t_1}\right)^{\beta} \exp\left[\beta \left(1 - \frac{\bar{t} - t_{m1}}{\Delta t_1}\right)\right], & \\ \qquad\qquad t_{m1} \le \bar{t} \le t_{m2} = t_{m_1} + \Delta t_1, & \\ T_{high}^{\pm}, \quad t_{m2} \le \bar{t} \le t_{m3} = t_{m_2} + \Delta t_2, & \\ T_{low}^{\pm} + (T_{high}^{\pm} - T_{low}^{\pm}) \left(\frac{\bar{t} + \Delta t_1 - t_{m3}}{\Delta t_1}\right)^{\beta} \exp\left[\beta \left(1 - \frac{\bar{t} + \Delta t_1 - t_{m3}}{\Delta t_1}\right)\right], & \\ \qquad\qquad t_{m3} \le \bar{t} \le t_{m4} = t_{m_3} + \Delta t_3, \Delta t_1 \ll \Delta t_3, & \\ T_{low}^{\pm}, \quad t_{m4} \le \bar{t} \le t_{m5}, & \end{cases} \tag{2.9}$$

where $T_{low}^{\pm}$ and $T_{high}^{\pm}$ are low and high transmittance of the Q-switch, time moments are given by relations

$$t_{mj+1} = t_{mj} + \Delta t_j, j = 1, \ldots, 4,\ t_{mj} = t_{0j} + m\Delta t, \Delta t = \sum_j \Delta t_j, m = 0, 1, \ldots$$

and coefficient $\beta = 1, 2, \ldots$ determines the steepness of the pulse fronts.

Propagation through passive elements and free space. The pulse propagation in passive optical elements (and in free space also) is described by simple transport equations

$$\frac{1}{v_e} \frac{\partial I_e^{\pm}}{\partial t} \pm \frac{\partial I_e^{\pm}}{\partial z} = 0. \tag{2.10}$$

Initial and boundary conditions. For AE placed between $z_1^{AE} \le z \le z_2^{AE}$ equations (2.1), (2.2), (2.3), (2.4)–(2.7) are solved in this interval only. It is commonly assumed that $N_1(z, t = 0) = N_{Nd}$ and $N_j(z, t = 0) = 0$, $j = 2, 3, 4$. It is also assumed that at initial moment the laser and pump waves are absent in the region $z_1^{AE} \le z \le z_2^{AE}$, that is $I^{\pm}(z, t = 0) = 0$ and $I_{p1,2}^{\pm}(z, t = 0) = 0$. Boundary conditions for laser waves are given by

$$I^{+}(z = 0, t) = R_1 I^{-}(z = 0, t) + I_{seed}^{+}(z = 0, t),$$
$$I^{-}(z = L, t) = R_2 I^{+}(z = L, t) + I_{seed}^{-}(z = L, t)$$

and for pump waves

$$I^{+}_{p1,2}(z=0,t) = (1-R_1^{(p1,2)})I^{-}_{p1,2}(z=0,t),$$
$$I^{-}_{p1,2}(z=Z_{p1,2},t) = R_2^{(p1,2)}I^{+}(z=Z_{p1,2},t)$$

In these expressions R_1 and R_2 are the reflection coefficients of resonator mirrors, $R_1^{(p1,2)}$ is the reflection coefficient of the front resonator mirror at pump wavelength $\lambda_{p1,2}$. $R_2^{(p1,2)}$ is the reflection coefficient of the additional dichroic mirror after the AE for reflection of pump wave into AE.

It should be noted that at all interfaces $z = z_A$ inside the resonator the incident and transmitted intensities are assumed to be equal

$$I^{\pm}(z_A \mp 0, t) = I^{\pm}(z_A \pm 0, t).$$

For simplicity we assume that all seed and pump intensities have the same functional form as transmittance function (2.9) with different quantitative parameters.

3 Simulation Results and Discussion

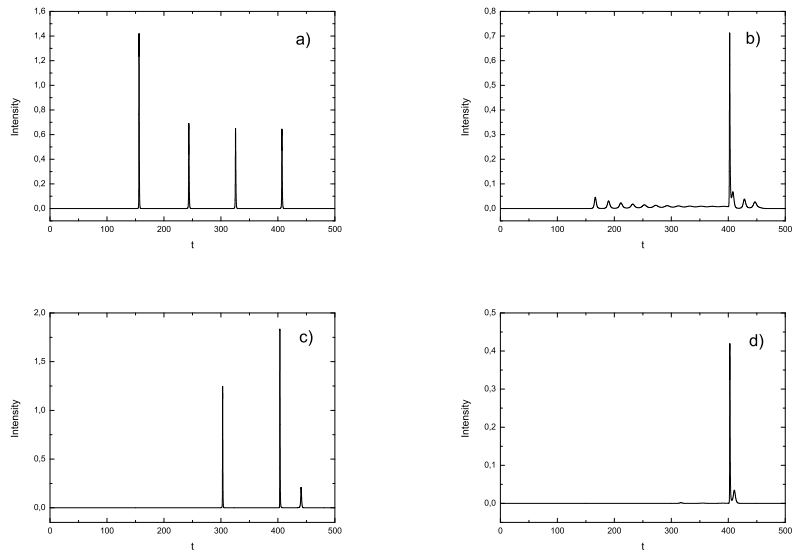

Figure 4. Generation dynamics using a) passive, b) active, c) active-passive, d) passive-active Q-switching.

In this paper we present results which first of all show the principal difference between results obtained using laser TWM and PLM. It is obvious that the results of TWM may depend on the optical elements sequence inside the resonator. The situation is different for PLM in which we cannot distinguish

different element sequences because of the averaging procedure along the resonator. For numerical solution of transport equations (2.1), (2.2), (2.3), (2.8) and (2.10) the algorithm developed in [11, 23] was used. Fig. 4 shows the positive-traveling (toward the front mirror with reflection coefficient R_2) laser pulses generated when only AQS is turned on Fig. 4a, only PQS is turned on Fig. 4b, both passive and active Q-switches are turned on together Fig. 4c, and active Q-switch precedes the passive one Fig. 4d. PQS has initial transmittance about 10%, that is $N_{Cr}^{(j)} = 0.719$ for 1 mm thick Cr:YAG crystal with $\sigma_g = 32$ and $\sigma_e = 2.8$. The conducted simulations show that the results depend only slightly on the values of relaxation times τ_{32} and τ_{a21}. They influence pulse repetition rate only. Therefore, in order to reduce the simulation time, we have used shorter durations of relaxation times τ_{32}, τ_{a21} and higher pump intensities as compared with a real experimental situation for laser diode pumped Nd:YAG lasers. To obtain results shown in Fig. 4, we have used the following values: $\tau_{32} = 500$, $\tau_{a21} = 100$, $R_1 = 1.0$ and $R_2 = 0.2$. Active Q-switch has following transmittances $T_{low}^{\pm} = 0.1$, $T_{high}^{\pm} = 0.95$ and enough long switching on time $\Delta t_1 = 10$ with steepness coefficient $\beta = 2$. It can be seen that for similar transmittance parameters of passive and active Q-switches the generation dynamics is different. During PQS a sequence of pulses is generated. Using AQS with high enough initial transmittance the so called relaxation oscillations are observed before it is turned on to the high transmittance. After the AQS is opened, the giant pulse is generated. As expected, results of combined passive and active Q-switching depend on the chain of these elements in the resonator.

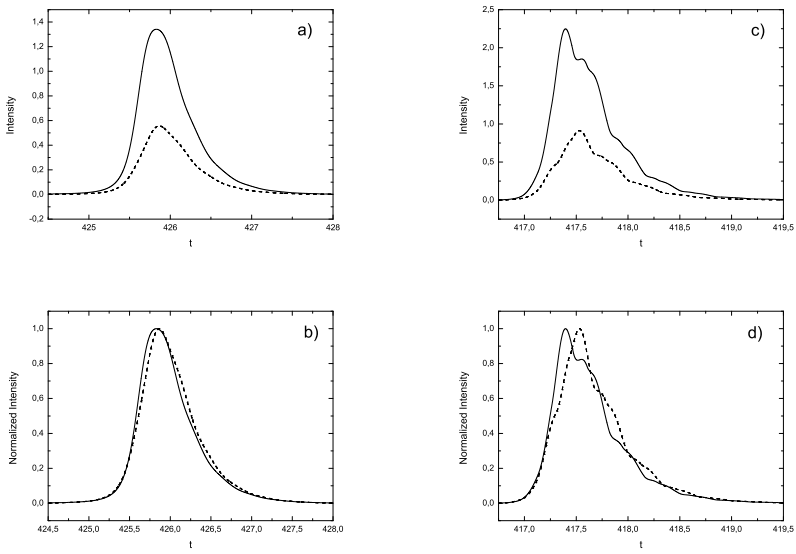

Figure 5. Shapes of forward (+) and backward (-) traveling pulses inside the resonator before the outgoing mirrors using passive (a, b) and active (c, d) Q-switching.

Using TWM we can expect that for outgoing pulses through the front and

rear mirrors not only amplitudes of pulses but also their shapes may be different. Fig. 5 shows pulse shapes using active and passive Q-switching separately. It is seen that amplitudes of pulses inside the resonator differ very strongly. This difference increases even more when pulses pass the output mirrors with reflection coefficients $R_1 = 0.9$ and $R_2 = 0.2$ because the transmitted intensities and pulse energies are given by expressions

$$W_{1m} = \int_{t_{m0}}^{t_{m0}+\Delta t} (1 - R_1) I^-(t)\, dt, \quad W_{2m} = \int_{t_{m0}}^{t_{m0}+\Delta t} (1 - R_2) I^+(t)\, dt.$$

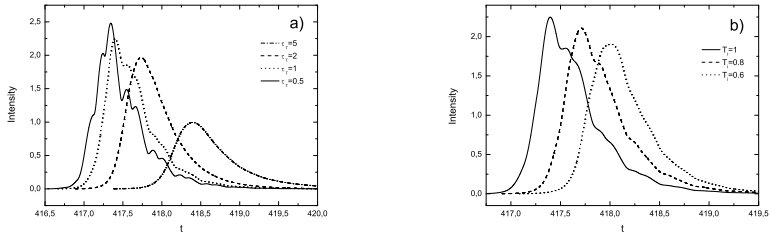

Figure 6. Temporal pulse modulation a) in the case of high rate opening of AQS, b) pulse shape smoothing by additional PQS with high enough transmittance.

It is also seen from the normalized intensities that shapes of forward and backward traveling pulses differ only slightly for PQS. Unlike PQS we can control the rate of AQS. It is seen that for fast enough Q-switching with leading front rising time $\tau_T = \Delta t_1 = 1$ (see, Fig. 5c,d) the shapes of generated pulses have temporal modulation with period shorter than resonator round-trip time. We think that this modulation is caused by strong and fast modulation of pulse amplitudes inside the resonator by the AQS and low reflection coefficient of front mirror. Influence of the switching rate on pulse shape and amplitude can be seen from Fig. 6a. For low switching rate ($\tau_T = 5$ and $\tau_T = 2$) the generated pulses have smooth shapes but are less intensive as compared with fast switching. Thus, using slow active switching the smooth pulses with significantly lower energy are generated. Pulse smoothing with higher efficiency can be realized by the use of additional PQS with high enough initial transmittance T_i. This possibility is demonstrated in Fig. 6b, where the pulse shapes are obtained by simultaneous usage of AQS with $\tau_T = 1$ and PQS with different initial transmittance. It should be noted that in our simulations turning out of PQS means that $N_{Cr} = 0$, i.e. its initial and final transmittance are equal to $T_i = T_f = 1$. Thus, the optical path of the resonator does not change during such turnings on/off of PQS. Therefore, the condition of generation remains the same in both cases, and there are no causes to generate shorter pulses.

The developed software allows us to control temporal changes of investigated variables in different planes along the resonator. From Fig. 7 we can see how the population densities of AE laser working manifolds and of SA are changing during the generation of giant pulses by PQS. It is seen that bleaching of SA

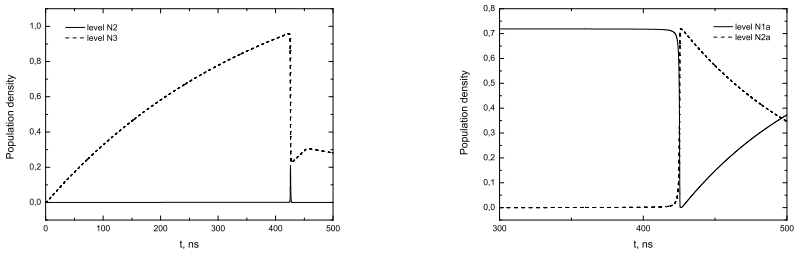

Figure 7. Temporal changes of population densities in AE and pQ-sw during the pumping and pulse generation.

is smooth but very fast. Therefore, for generating smooth pulses by AQS its opening should be fast and smooth simultaneously.

We can also control the spatial changes (along the resonator) of studied quantities at different predetermined times, e.g. before, in time and after of giant pulse generation. Fig. 8 presents changes along the AE of the population densities (Fig. 8a,c) and changes of the pumping intensities (Fig. 8b,d) at time moments just before the generation of giant pulses using PQS for different kinds of pumping: indirect – through the pump levels (Fig. 8a,b) and direct – to the upper laser manifold (Fig. 8c,d). It can be seen from equations (2.1), (2.2) that for the low pump intensities, when population densities $N_3 \approx 0$ and $N_4 \approx 0$, the pump absorption coefficients are equal to

$$\tilde{\alpha}_{1p} \approx \sigma_p^{(14)} f_{1p}^{(14)} N_1 \approx \sigma_p^{(14)} f_{1p}^{(14)} N_{Nd}, \qquad (3.1)$$
$$\tilde{\alpha}_{2p} \approx \sigma_p^{(13)} f_{1p}^{(13)} N_1 \approx \sigma_p^{(13)} f_{1p}^{(13)} N_{Nd}.$$

Due to short relaxation times from pump level manifold (we used in our calculations $\tau_{43} = 0.3$) the pumping manifold is not populated ($N_4 \approx 0$) and the formula (3.1) is good enough for high pumping intensities too. Therefore, the saturation of absorption does not occur practically. This statement is confirmed by Fig. 8b. It is seen that absorption of the pump does not differ for the cases with and without reflection mirror. It is seen also that absorption of the pump is low enough ($\tilde{\alpha}_1 \approx 0.95$). Therefore, the additional mirror for pump backward reflection after the AE increases the population of upper laser manifold significantly (Fig. 8a).

The situation with pump saturation is different for direct pumping. It is seen from Fig. 8d that absorption of pump intensity is higher in the absence of reflection mirror. Experimental values of spectroscopic cross section σ_p^{13} and σ_p^{14} are not known exactly. Therefore, we have used the same value (0.4) for both of them. Due to lower absorption coefficient for this case the population density is practically homogeneous along the AE (Fig. 8c) when additional reflection mirror for pump intensity is used.

Thus, it follows from obtained results that distribution of population densities is inhomogeneous along the AE, especially for high enough pump absorption. The same statement is even more significant to the spatial distribution

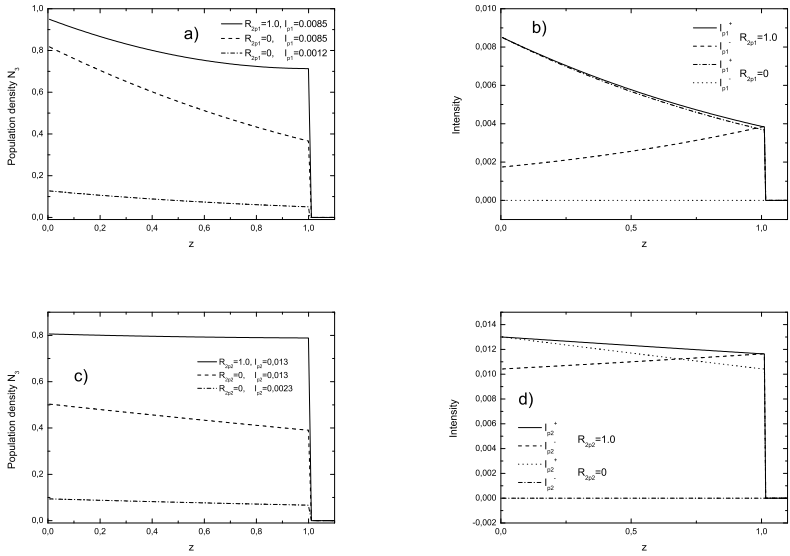

Figure 8. Spatial dependences (along the AE) of the population densities N_3 and pump intensities I_p for the indirect a, b and direct c, d pumping.

along the resonator of the intensity of generated laser pulse. Fig. 9 presents the spatial behaviour of PQS generated laser pulse inside the resonator at the moment of its maximum intensity. It is seen that spatial changes of pulse intensity are very strong. First of all, the intensity of the forward and backward traveling pulse strongly increases during propagation (amplification) inside the AE ($0 \le z \le 1$). Then, it is seen that even at the moment of pulse maximum the absorption in PQS ($1 \le z \le 1.1$) is noticeable due to excited state absorption. During the free propagation in other passive elements of the resonator the changes of pulse intensities are small because the spatial length of the generated pulses is much longer than the length of resonator. Therefore, spatially averaged intensity cannot show in general case the true situation inside the SSL resonator. Thus, PLM cannot be used for generation dynamics description when the traveling laser waves are subjected to the strong impact from the active and passive elements inside the resonator.

4 Conclusions

Traveling wave model (TWM) is used for detailed numerical analysis of generation dynamics of laser diode end-pumped solid-state lasers with active and passive Q-switching. In addition to standard indirect pumping through he pump manifold, the Stark splitting and Boltzmann occupation factors of active ions energy levels gives the possibility to use direct resonant pumping into upper laser working manifold, short and long relaxation times from excited levels, excited state absorption in active element and passive Q-switch and other

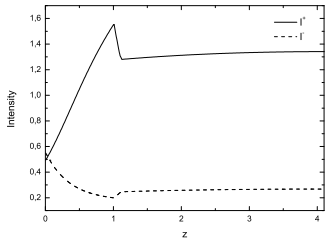

Figure 9. Spatial distribution of laser pulse intensity along the AE at the moment of maximum intensity of outgoing laser pulse.

processes, such as energy transfer upconversion are taken into account.

It is shown that generation dynamics depends on element distribution inside the resonator, that is a TWM, unlike widely used point laser model, can take a proper account of element layout in the resonator. The pulse shapes of outgoing pulses through the front and rare mirrors differ visibly, especially for fast change of transmittance of active Q-switch. For this case the generated pulses have temporal modulation with typical times shorter than resonator roundtrip time. This temporal modulation can be smoothed by using an additional passive Q-switch element with enough high initial transmittance without significant decrease of pulse energy. Developed software allows us to control temporal and spatial distributions of pump and laser intensities, population densities and other parameters inside the resonator. Usage of traveling wave model for the description of pump absorption allows us to observe the saturation of pump absorption, which is especially significant for direct resonant pumping.

It is shown that intensity distributions of the forward and backward traveling generated laser pulses inside the resonator are strongly spatially modulated. Therefore, we think that the standard point laser model cannot give correct results in the situations when traveling waves inside the resonator are subjected to strong impact from active and passive elements of resonator and as a result acquire sharp and strong changes of intensities.

Acknowledgment

One of the authors (ASD) would like to thank the Agency for International Science and Technology Development Programmes in Lithuania for support within the Eureka project E!3765 EULASNET II.

References

[1] V.V. Antsiferov and G.I. Smirnov. *Physics of solid-state lasers.* Cambridge International Science Publishing Ltd, 2005.

[2] F. Bachmann, P. Loosen and R. Poprawe(Eds.). *High power diode lasers: Technology and Applications.* Springer, New York, 2007.

[3] N. P. Barnes. Solid-state lasers from efficiency perspective. *IEEE J. Sel. Top. Quantum Electron*, **13**(3):435–447, 2007. Doi:10.1109/JSTQE.2007.895280.

[4] S.A.van den Berg, G.W. 't Hooft and E. R. Eliel. Pulse-train formation in a gain-switched polymer laser resulting from spatial gain inhomogeneity. *Phys. Rev. A.*, **63**(6), 2001. Doi:10.1103/PhysRevA.63.063809.

[5] S. Biswal, J. Itatani, J. Nees and G.A. Mourou. Efficient energy extraction below the saturation fluence in loqw-gain low-loss regenerative chierped-pulse amplifier. *IEEE J. Sel. Top. Quantum Electron*, **4**(2):421–425, 1998. Doi:10.1109/2944.686750.

[6] J.L. Blows, G.W. Forbes and J.M. Dawes. Cavity modes in diode-array end-pumped planar lasers with aberrated thermal lenses. *Opt. Commun.*, **186**(1):111–120, 2000. Doi:10.1016/S0030-4018(00)01057-9.

[7] D. C. Brown and J. W. Kuper. Solid-state lasers: Steady progress through the decades. *OPN*, **20**(5):37–41, 2009.

[8] R. Buzelis, A. Dement'ev, E. Kosenko, E. Murauskas, R. Čiegis and G. Kairytė. Numerical analysis and experimental investigation of beam quality of SBS-compressors with multipass Nd:YAG amplifier. *Laser Optics' 95: Solid State Lasers, A.A.Mak, V.I.Ustyugov, Editors, Proc. SPIE*, **2772**:158–169, 1996.

[9] R. Buzelis, A. Dement'ev, E. Kosenko, E. Murauskas, R. Navakas and M. Radziunas. Generation of short pulses with low jitter in combined actively and passively Q-switched solid-state laser with short resonator. *Lithuanian Phys. J.*, **38**(3):248–257, 1998.

[10] R. Buzelis, A. Dement'ev, E. Kosenko, E. Murauskas, R. Vaicekauskas and F. Ivanauskas. Amplification efficiency and quality alteration of short pulses amplified in the Nd:YAG amplifier in the saturation mode. *Lithuanian Phys. J.*, **38**(4):289–301, 1998.

[11] R. Čiegis, A. Dement'ev and I.Laukaitytė. Numerical algorithm for simulation of the Q-switched fiber laser using travelling wave model. *Lithuanian Math. J.*, **48**(3):270–281, 2008. Doi:10.1007/s10986-008-9011-y.

[12] R. Čiegis, M. Radziunas and M. Lichtner. Numerical algorithms for simulation of multisection lasers by using traveling wave model. *Math. Model. Anal.*, **13**(3):327–348, 2008. Doi:10.3846/1392-6292.2008.13.327-348.

[13] A. Dement'ev, E. Kosenko and R. Navakas. Investigation of bleaching of Cr4+:YAG crystals by laser pulses of different duration and nonhomogeneous transverse intensity distribution. *Lithuanian Phys. J.*, **39**(4):263–272, 1999.

[14] A. Dement'ev and R. Navakas. Modeling of generation of solid-state minilasers with combined active-passive Q-switching and diode pumping. *Lithuanian Phys. J.*, **39**(6):392–401, 1999.

[15] A. Dement'ev and R. Navakas. Some aspects of the inverse problem of Cr^{4+}:YAG absorption cross sections using experimental data of transmission. *Nonlinear Analysis: Modelling and Control*, **6**(1):39–55, 2001.

[16] A. Dement'ev, R. Navakas and R. Vaicekauskas. Modeling of generation dynamics of passively and actively Q-switched solid-state lasers. *Math. Model. Anal.*, **5**:32–43, 2000.

[17] J. C. Diels and W. Rudolph. *Ultrafast Laser Pulse Phenomena*. Sec. Ed. Academic Press, Amsterdam, 2005.

[18] M. Eichorn. Quasi-three-level solid-state lasers in the near and mid infrared based on trivalent rare earth ions. *Appl. Phys. B.*, **93**(2):269–316, 2008. Doi:10.1007/s00340-008-3214-0.

[19] A. K. Jafari and M. Aas. Continuous-wave theory of Yb:YAG end-pumped thin-disk lasers. *Appl. Opt.*, **48**(1):106–113, 2009. Doi:10.1364/AO.48.000106.

[20] J. Javaloyes and S. Balle. Emission directionality of semiconductor ring lasers: a traveling-wave description. *IEEE J. Quantum Electron*, **45**(5):431–438, 2009. Doi:10.1109/JQE.2009.2014079.

[21] Ya.I. Khanin. *Principles of laser dynamics*. Elsevier Science B.V., Amsterdam, 1995.

[22] J. W. Kim, J. I. Mackenzie and W. A. Clarkson. Influence of energy-transfer-upconversion on the threshold pump power in quasi-three-level solid-state lasers. *Opt. Exp.*, **17**(14):11935–11943, 2009. Doi:10.1364/OE.17.011935.

[23] I. Laukaitytė and R. Čiegis. Finite-difference scheme for one problem of nonlinear optics. *Math. Model. Anal.*, **13**(2):211–222, 2008. Doi:10.3846/1392-6292.2008.13.211-222.

[24] C. Lim and Y. Izawa. Modeling of end-pumped CW quasi-three-level lasers. *IEEE J. Quantum Electron*, **38**(3):803–811, 2002.

[25] W.H. Lowdermilk and J. E. Murray. The multipass amplifier: Theory and numerical analysis. *J. Appl. Phys.*, **51**(5):2436–2444, 1980. Doi:10.1063/1.328014.

[26] A. L. Mikaelyan, M. L. Ter-Mikaelyan and Yu.G. Turkov. *Optical Solid-State Generators*. Sov. Radio, Moscow, 1967.

[27] S. Pearce, C. L. M. Ireland and P. E. Dyer. Simplified analysis of double-pass amplification with pulse overlap and application to nd:yvo4 laser. *Opt. Commun.*, **255**(4):297–303, 2005. Doi:10.1016/j.optcom.2005.06.013.

[28] D. Sangla, F. Balembois and P. Georges. Nd:YAG laser diode-pumped directly into the emitting level at 938 nm. *Opt. Exp.*, **17**(12):10091–10097, 2009. Doi:10.1364/OE.17.010091.

[29] S. Schwartz, G. Feugnet, M. Rebut, F. Bretenaker and J-P. Pocholle. Orientation of Nd^{3+} dipoles in yttrium aluminum garnet: Experimental and model. *Phys. Rev. A.*, **79**:39–55, 2009. Doi:10.1103/PhysRevA.79.063814.

[30] A. Sennaroglu(Ed.). *Solid–State Lasers and Applications*. CRC Press, London, 2007.

[31] L.V. Tarasov. *Physics of Processes in Coherent Optical Radiation Generators*. Radio i Svyaz', Moscow, 1982.

[32] P.P. Vasil'ev, I. H. White and J. Gowar. Fast phenomena in semiconductor lasers. *Rep. Prog. Phys.*, **63**(12):1997–2042, 2000. Doi:10.1088/0034-4885/63/12/203.

[33] Y. Wang and C-Q. Xu. Actively Q-switched fiber lasers: switching dynamics and nonlinear processes. *Prog. Quantum Electron*, **31**(3):131–216, 2007. Doi:10.1016/j.pquantelec.2007.06.001.

[34] M. Wohlmuth, C. Pflaum, K. Altmann, M. Paster and C. Hahn. Dynamic multimode analysis of Q-switched solid state laser cavities. *Opt. Exp.*, **17**(20):17303–17316, 2009. Doi:10.1364/OE.17.017303.

[35] J. Zayhowski, D. Welford and J. Harrison. Miniature solid-state lasers. In M. C. Gupta and C. Ballato(Eds.), *Handbook of Photonics. Second edition*, pp. 10.1–10.98. CRC Press, New York, 2007.

[36] G.M. Zverev and Yu.D. Golyaev. *Crystal Lasers and Their Applications*. Radio i Svyaz', Moscow, 1994.